DOI: 10.1016/j.apenergy.2019.04.067

Advancements on scaling-up simulation of Proton Exchange Membrane Fuel Cells impedance through Buckingham Pi theorem[1]

Pierpaolo Polverino[*,a], Giovanni Bove[a], Marco Sorrentino[a], Cesare Pianese[a], Davide Beretta[b]

[a] *Department of Industrial Engineering, University of Salerno, via Giovanni Paolo II 132, 84084, Fisciano (SA), ITALY.*

[b] *European Institute for Energy Research (EIFER), Emmy-Noether Strasse 11, D-76131, Karlsruhe, GERMANY.*

[*]Corresponding author: e-mail ppolverino@unisa.it, Tel. +39 089 96 4178, Fax. +39 089 96 4037.

Abstract

This paper addresses a generalized scaling-up technique applied to Proton Exchange Membrane Fuel Cells (PEMFCs). This methodology allows simulating the impedance related to a full stack from that of a single cell or short stack, combining experimental data with physical reasoning and phenomenological modelling. The use of such technique can reduce Electrochemical Impedance Spectroscopy (EIS) testing costs, with a significant impact on fuel cell manufacturing and performance assessment processes. The procedure described in this paper relies on a former approach, already presented by the authors, which has been improved with respect to two main aspects. Firstly, non-dimensional parameters are computed through a generalized physical model. Secondly, single cell or short stack internal states (i.e., water content and limiting current) are evaluated through significant information gained from impedance measurements and inverse modelling. Stack impedance simulation is performed through proper internal states distribution assumptions. To prove the consistency and robustness of the proposed technique, experimental data taken from the literature and the European funded project HEALTH-CODE are used, with stack impedance accurately reproduced by means of only a single cell spectrum.

Keywords: Buckingham theorem; similarity; scaling-up; modelling; Electrochemical Impedance Spectroscopy; Proton Exchange Membrane Fuel Cell.

1. Introduction

[1] The short version of the paper was presented at the 10th International Conference on Applied Energy (ICAE2018), 22-25 August 2018, Hong Kong, China. This paper is a substantial extension of the short version of the conference paper.

The current advancements in materials design and components manufacturing brought Proton Exchange Membrane Fuel Cell (PEMFCs) technology to affirm itself as one of the most promising energy conversion systems, both for stationary [1], even in reversible operation [2], and transport applications [3]. Nevertheless, there are still significant barriers to be overcome to finally establish PEMFC mass market penetration, such as the high production and operating costs [4], limited durability, with respect to the reference targets [5][6], and the need for ensuring satisfactory performance throughout its lifetime.

With the aim of providing acceptable and cost-effective solutions to attain the best compromise among the aforementioned conflicting goals, current research and industrial efforts mostly focus on manufacturing processes improvement, as well as developing effective control, diagnostic and prognostic strategies. The manufacturing process of PEMFC stacks generally consists of the following steps: (i) single cells production, (ii) stack assembly and (iii) stack testing and conditioning [7]. Each of the cited steps has a precise cost, depending on consumed materials as well as manufacturing procedures time and scheduling. As pointed out by a cost analysis performed by the Battelle Institute for the U.S. Department of Energy in 2016 [7], testing and conditioning costs may vary between 4% (100 produced units) and 1.6% (50'000 produced units) of the total cost of a 60 kW stack for stationary applications (i.e., backup or combined heat and power – CHP – uses). Dedicated devices are needed for stack testing, which should correctly perform stack conditioning and performance assessment, in order to evaluate stack quality and its suitability for system integration. Clearly, the choice of the device type, amount of reactants and time required for the stack testing depend on its size, influencing the overall test and conditioning procedure costs.

As for durability and efficient working throughout system lifetime, suitable diagnostic algorithms coupled with efficient control strategies can be adopted [8]. The proper combination of diagnostics and control can promptly act to prevent fault worsening, so as to reduce system degradation or avoid any abrupt failure, and thus improve system durability and lifetime [9]. In the literature, it emerges how several researchers exploited Electrochemical Impedance Spectroscopy (EIS) to develop effective diagnostic procedures for PEMFC systems. Particularly, faults can be detected, using the EIS, by recording impedance spectra during fuel cell operation and then analyzing these data using the Equivalent Circuit Modelling (ECM) approach with diagnostic purposes [10][11]. The paper of Narjis et al. [12] provides the main references for the development of fault detection and isolation (FDI) based on EIS. Moreover, the use of more physical-based

modelling representation of fuel cell impedance has been thoroughly accounted for in the literature. For example, Kulikovsky proposed the analytical model of a PEMFC cathode catalyst layer impedance, under poor oxygen transport [13][14] and at open circuit voltage in addition to the Gas Diffusion Layer impedance [15]. The work of Cruz-Manzo et al. [16] describes the PEMFC impedance spectra subject to Pt oxidation and H_2 peroxide formation at cathode side, whose information were suitably combined with those retrievable from physical and circuit modelling. On the same line, Cruz-Manzo et al. [16] and Niya et al. [17] developed an impedance model combining physical and ECM approaches, particularly aiming at describing a PEMFC impedance at different operating conditions, varying current densities, temperature and humidity levels. Physics-based PEMFC impedance models were also developed by Setzler and Fuller [18], with the implementation of an oxide growth oxygen reduction reaction kinetic model, and Chevalier et al. [19][20], aiming at PEMFC state-of-health and degradation analysis. The analysis of the cells output voltage signal with discrete wavelet transform (DWT) and continuous wavelet transform (CWT) were also proposed for fuel cells FDI in the recent literature [21].

Nevertheless, traditional EIS equipment is expensive, bulky and requires several minutes to perform a single impedance spectrum measurement [22]. Moreover, the diagnosis can be performed once some metrics are derived through EIS signal treatment [23]. The scaling-up approach introduced in a previous authors' work [24] offers an innovative methodology to reduce stack testing costs and cope with the afore-mentioned EIS limitations. Such an approach particularly allows stack performance estimation by scaling-up in size the performance of a single cell or a short stack from the same technology. Through this advantage, a direct testing of full stack is no more necessary and, thus, a smaller testing device type and less reactants are needed. Nonetheless, the main limit related to the proposed approach consists in the use of non-general models to be identified over tested technologies before performing scaling-up. This implies the need for a great amount of experimental data that could be difficult to retrieve or are not yet available, in the case of new technologies. Moreover, the states of single cell/short stack internal variables (such as humidity, reactants distribution, etc.) to be scaled-up is assumed known according to hypothetical reasoning, without any estimation, with consequent reduction in performance assessment robustness.

To overcome the aforementioned limitations, an improved methodology is here illustrated, remarking two key features: (i) a more generalized modelling framework is adopter so as to reduce methodology

dependence on experimental data, and (ii) single cell internal states are identified from available experimental data (used for the scaling-up approach) through inverse modelling. The paper is thus structured as follows: an overview of the scaling-up methodology is firstly given, followed by the detailed description of the newly introduced sub-models of electrolyte and polarization resistance. Afterwards, the genericity and accuracy guaranteed by the updated version of the Buckingham-based modeling and scaling-up procedure are experimentally verified, by reproducing EIS spectra in several operating conditions and for different PEMFC stacks. Finally, the concluding remarks are given, aiming at emphasizing the main contributions provided, as well as underlining what the most significant expected real-world implications will be.

2. Overview of the scaling-up approach

The approach for PEMFC impedance scaling-up described in this paper has been initially investigated by the authors in [24] and further generalized in [25]. A short introduction on the theoretical basis the approach is developed on is here given for the sake of clarity. The approach relies on the Buckingham's Pi Theorem, which allows defining correlations among variables of a specific physical problem by means of their dimensional analysis. The aim of such theorem is to defined significant non-dimensional parameters, which can be representative of the considered problem and can be used to scale-up the involved variables upon specific physical assumptions.

2.1. The Buckingham Pi Theorem

Given a specific physical problem involving n variables, let x_0 be a dependent variable that can be expressed as function of the remaining n-1 independent variables (x_1 through x_{n-1}):

$$x_0 = f\left(x_1,...,x_{n-1}\right) \tag{1}$$

Defining v as the number of all the involved fundamental dimensions related to the n variables, let k be the minimum number of variables dimensionally independent, through which the dimensions of all remaining variables can be constructed (with $k \leq v$) [26]. From the dimensional analysis of such variables, a certain number p of non-dimensional parameters π_i (with i = 0 to p-1) can be defined as [24]:

$$p = n - k \tag{2}$$

Such parameters can be expressed as the ratio between the remaining p variables (i.e., those not included in the k subset) and the product of the chosen k variables, raised to an exponent α_{ij} (with j = 1 to k) that brings to zero the dimension of the parameters:

$$\pi_i = \frac{x_i}{\prod_{j=1}^{k} x_j^{\alpha_{ij}}} \tag{3}$$

The non-dimensional parameter π_0 is the one related to the dependent variable x_0 and can be expressed as function of all the other p-1 non-dimensional parameters [24]:

$$\pi_0 = g\left(\pi_1, ..., \pi_{p-1}\right) \tag{4}$$

The Buckingham's Pi Theorem is here applied to identify non-dimensional parameters linking the impedance of a PEMFC to electrochemical and physical variables.

2.2. Problem formulation and non-dimensional parameters definition

The impedance Z of a PEMFC generally depends on the operating conditions at which the measurement is performed and it represents an indicator of the main electrochemical features of the fuel cell. Therefore, it can be expressed as function of operating variables (e.g., current I, temperature T_{fc} and frequency ω) and electrochemical parameters (such as equivalent cell resistance R_{eq}, capacitance C, and electrochemical surface area A_{fc}). The problem can be thus formulated as follows:

$$Z = f\left(I, T_{fc}, \omega, R_{eq}, C, A_{fc}\right) \tag{5}$$

The problem shows n = 7 variables, with Z as the main dependent variable. According to the International System of Units [27], the involved fundamental dimensions are length [L], mass [M], time [T] electric current [I] and thermodynamic temperature [Θ]:

$$\begin{aligned}
\left[Z\right] &= \left[\mathrm{L}^2\mathrm{M}^1\mathrm{T}^{-3}\mathrm{I}^{-2}\Theta^0\right] \\
\left[I\right] &= \left[\mathrm{L}^0\mathrm{M}^0\mathrm{T}^0\mathrm{I}^1\Theta^0\right] \\
\left[T_{fc}\right] &= \left[\mathrm{L}^0\mathrm{M}^0\mathrm{T}^0\mathrm{I}^0\Theta^1\right] \\
\left[\omega\right] &= \left[\mathrm{L}^0\mathrm{M}^0\mathrm{T}^{-1}\mathrm{I}^0\Theta^0\right] \\
\left[R_{eq}\right] &= \left[\mathrm{L}^2\mathrm{M}^1\mathrm{T}^{-3}\mathrm{I}^{-2}\Theta^0\right] \\
\left[C\right] &= \left[\mathrm{L}^{-2}\mathrm{M}^{-1}\mathrm{T}^4\mathrm{I}^2\Theta^0\right] \\
\left[A_{fc}\right] &= \left[\mathrm{L}^2\mathrm{M}^0\mathrm{T}^0\mathrm{I}^0\Theta^0\right]
\end{aligned} \tag{6}$$

However, it is worth observing that the thermodynamic temperature appears only in the cell temperature dimension, and thus the related variable shall be removed from the analysis [28]. Therefore, the problem results in $n = 6$ variables with $v = 4$ fundamental dimensions:

$$\begin{aligned}
\left[Z\right] &= \left[\mathrm{L}^{2}\mathrm{M}^{1}\mathrm{T}^{-3}\mathrm{I}^{-2}\right] \\
\left[I\right] &= \left[\mathrm{L}^{0}\mathrm{M}^{0}\mathrm{T}^{0}\mathrm{I}^{1}\right] \\
\left[\omega\right] &= \left[\mathrm{L}^{0}\mathrm{M}^{0}\mathrm{T}^{-1}\mathrm{I}^{0}\right] \\
\left[R_{eq}\right] &= \left[\mathrm{L}^{2}\mathrm{M}^{1}\mathrm{T}^{-3}\mathrm{I}^{-2}\right] \\
\left[C\right] &= \left[\mathrm{L}^{-2}\mathrm{M}^{-1}\mathrm{T}^{4}\mathrm{I}^{2}\right] \\
\left[A_{fc}\right] &= \left[\mathrm{L}^{2}\mathrm{M}^{0}\mathrm{T}^{0}\mathrm{I}^{0}\right]
\end{aligned} \tag{7}$$

It can be observed from equation (7) that only two variables (i.e., Z and R_{eq}) are dimensionally dependent and it can be then assumed that $k = v = 4$. Among the possible independent subsets, the chosen one contains I, ω, R_{eq} and A_{fc}, and the remaining $p = n - k = 2$ variables are Z and C [25]. The two non-dimensional parameters are then evaluated as follows:

$$\pi_0 = \frac{Z}{I^{\alpha_{01}}\omega^{\alpha_{02}}R_{eq}^{\alpha_{03}}A_{fc}^{\alpha_{04}}} \tag{8a}$$

$$\pi_1 = \frac{C}{I^{\alpha_{11}}\omega^{\alpha_{12}}R_{eq}^{\alpha_{13}}A_{fc}^{\alpha_{14}}} \tag{8b}$$

The exponents α_{ij} in equation (8) are evaluated considering that the dimension of the parameters π_0 and π_1 is zero:

$$\left[\mathrm{L}^{0}\mathrm{M}^{0}\mathrm{T}^{0}\mathrm{I}^{0}\right] = \frac{\left[\mathrm{L}^{2}\mathrm{M}^{1}\mathrm{T}^{-3}\mathrm{I}^{-2}\right]}{\left[\mathrm{L}^{0}\mathrm{M}^{0}\mathrm{T}^{0}\mathrm{I}^{1}\right]^{\alpha_{01}}\left[\mathrm{L}^{0}\mathrm{M}^{0}\mathrm{T}^{-1}\mathrm{I}^{0}\right]^{\alpha_{02}}\left[\mathrm{L}^{2}\mathrm{M}^{1}\mathrm{T}^{-3}\mathrm{I}^{-2}\right]^{\alpha_{03}}\left[\mathrm{L}^{2}\mathrm{M}^{0}\mathrm{T}^{0}\mathrm{I}^{0}\right]^{\alpha_{04}}} \tag{9a}$$

$$\left[\mathrm{L}^{0}\mathrm{M}^{0}\mathrm{T}^{0}\mathrm{I}^{0}\right] = \frac{\left[\mathrm{L}^{-2}\mathrm{M}^{-1}\mathrm{T}^{4}\mathrm{I}^{2}\right]}{\left[\mathrm{L}^{0}\mathrm{M}^{0}\mathrm{T}^{0}\mathrm{I}^{1}\right]^{\alpha_{11}}\left[\mathrm{L}^{0}\mathrm{M}^{0}\mathrm{T}^{-1}\mathrm{I}^{0}\right]^{\alpha_{12}}\left[\mathrm{L}^{2}\mathrm{M}^{1}\mathrm{T}^{-3}\mathrm{I}^{-2}\right]^{\alpha_{13}}\left[\mathrm{L}^{2}\mathrm{M}^{0}\mathrm{T}^{0}\mathrm{I}^{0}\right]^{\alpha_{14}}} \tag{9b}$$

From equation (9), the following systems are established and solved to find the required exponents:

$$\begin{cases}
2 - 2\alpha_{03} - 2\alpha_{04} = 0 \\
1 - \alpha_{03} = 0 \\
-3 + \alpha_{02} + 3\alpha_{03} = 0 \\
-2 - \alpha_{01} + 2\alpha_{03} = 0
\end{cases} \Rightarrow \begin{cases}
\alpha_{01} = 0 \\
\alpha_{02} = 0 \\
\alpha_{03} = 1 \\
\alpha_{04} = 0
\end{cases} \tag{10a}$$

$$\begin{cases} -2-2\alpha_{13}-2\alpha_{14}=0 \\ -1-\alpha_{13}=0 \\ 4+\alpha_{12}+3\alpha_{13}=0 \\ 2-\alpha_{11}+2\alpha_{13}=0 \end{cases} \Rightarrow \begin{cases} \alpha_{11}=0 \\ \alpha_{12}=-1 \\ \alpha_{13}=-1 \\ \alpha_{14}=0 \end{cases} \tag{10b}$$

In conclusion, the following non-dimensional parameters are defined [25]:

$$\pi_0 = \frac{Z}{R_{eq}} \tag{11a}$$

$$\pi_1 = \omega C R_{eq} \tag{11b}$$

which are related together as follows, as also stated in equation (4) [26][28]:

$$\pi_0 = g(\pi_1) \Rightarrow \frac{Z}{R_{eq}} = g(\omega C R_{eq}) \tag{12}$$

2.3. Impedance scaling-up

To achieve the scaling-up of a PEMFC impedance from a smaller unit of the same technology (e.g., a single cell, a short stack or a single repeated unit) up to a full stack, let the reference unit be labelled as *ref* and the full stack as *stk*. Then, equation (12) applies to both problems:

$$\frac{Z_{ref}}{R_{eq,ref}} = g(\omega_{ref} C_{ref} R_{eq,ref}) \tag{13a}$$

$$\frac{Z_{stk}}{R_{eq,stk}} = g(\omega_{stk} C_{stk} R_{eq,stk}) \tag{13b}$$

Since single cells are connected in series within the stack, the whole stack resistance is proportional to the cells number (i.e., $R_{eq,stk} \sim N_c$) whereas the stack capacitance has an inverse correlation with it (i.e., $C_{stk} \sim 1/N_c$). Therefore, if the same frequency range is considered (which usually happens when dealing with PEMFC impedance spectroscopy), then the following assumption can be made:

$$\frac{Z_{stk}}{R_{eq,stk}} \approx \frac{Z_{ref}}{R_{eq,ref}} \Rightarrow Z_{stk} = \frac{Z_{ref}}{R_{eq,ref}} R_{eq,stk} \tag{14}$$

allowing the scaling-up of stack impedance by the knowledge of its equivalent resistance $R_{eq,stk}$, and the impedance and equivalent resistance of the reference unit (Z_{ref} and R_{eq}, respectively). The reference impedance is considered acquired through dedicated measurements, but further information on the equivalent resistance shall be gathered.

3. Equivalent resistance modelling

As already presented in [24], the equivalent resistance R_{eq} can be modelled as the sum of two main contributions that are the electrolyte resistance R_e and the polarization resistance R_p:

$$R_{eq} = R_e + R_p \tag{15}$$

The electrolyte resistance is modelled following the work of Springer et al. [29]:

$$R_e = \frac{t_e}{\sigma_e}\frac{1}{A_{fc}} \tag{16}$$

with σ_e and t_e being the water conductivity and electrolyte thickness, respectively. The former parameter can be modelled as function of the average electrolyte water content λ according to the following equations [29]

$$\sigma_e = \left(0.005139\lambda - 0.00326\right)\exp\left[1268\left(\frac{1}{303} - \frac{1}{T_{fc}}\right)\right] \tag{17}$$

whereas the latter depends on the electrolyte dry thickness $t_{e,dry}$ and fractional change δ as follows [30]:

$$t_e = t_{e,dry}\left(1+\delta\right) \tag{18}$$

$$\delta = 1.41\cdot 10^{-2}\lambda^{1.1} - 1.37\cdot 10^{-4}\lambda^{2.4} \tag{19}$$

From a general point of view, the polarization resistance is mainly related to the electrochemical phenomena characterizing the activation and diffusion losses [31]. Therefore, it can be evaluated by the analysis of the voltage polarization V_p due to such phenomena [25]:

$$R_p = \frac{dV_p}{dI} \tag{20}$$

The term V_p can be further expressed as:

$$V_p = V_A + V_D \tag{21}$$

where V_A and V_D are the activation and diffusion polarizations, respectively [31]:

$$V_A = \frac{\hat{R}T_{fc}}{2\alpha F}\log\left(\frac{I}{I_0}\right) \tag{22}$$

$$V_D = \frac{\hat{R}T_{fc}}{2F}\log\left(\frac{I_L}{I_L - I}\right) \tag{23}$$

In equation (22), the terms $\hat{R}$, F, α and I_0 are the universal gas constant (8.314 J·mol^{-1}·K^{-1}), the Faraday's constant (96485 C·mol^{-1}), the charge transfer coefficient and the exchange current, respectively. The further term I_L in equation (23) is instead the limiting current. Therefore, the final model for the polarization resistance is [25]:

$$R_p = \frac{\hat{R}T_{fc}}{2F}\left(\frac{1}{\alpha I} + \frac{1}{I_L - I}\right) \tag{24}$$

Combining equations (16) and (24) into equation (15), the equivalent resistance can be defined. It is worth noting that such model can be applied to both single cell and full stack, but paying attention to the correct definition of the local states of each cell within the stack. Indeed, considering known the operating conditions at which a PEMFC stack operates (i.e., I and T_{fc}), defined the electrochemical and geometrical parameters (i.e., α, A_{fc} and $t_{e,dry}$), the remaining parameters still unknown are the electrolyte water content λ and the limiting current density I_L. Within the stack, these parameters can change from cell to cell, and their estimation is not easy to perform. Moreover, such parameters are hard to be defined through direct measurements and need to be carefully estimated, as described in the following.

3.1. Water content and limiting current density estimation

According to the approach proposed in [25], let R_{HF} and R_{LF} be the measured impedance values with zero imaginary part at high and low frequency, respectively. The former can be considered a rough estimation of the electrolyte resistance, whereas the latter of the whole equivalent resistance:

$$R_e \approx R_{HF} \tag{25}$$

$$R_{eq} \approx R_{LF} \tag{26}$$

Recalling equation (15), it can be also assumed that:

$$R_p = R_{eq} - R_e \approx R_{LF} - R_{HF} \tag{27}$$

Considering equations (16) through (19), equation (25) can be rewritten as:

$$\frac{\left(1+1.41\cdot10^{-2}\lambda^{1.1}-1.37\cdot10^{-4}\lambda^{2.4}\right)}{\left(0.005139\lambda-0.00326\right)} - \frac{A_{fc}R_{HF}}{t_{e,dry}}\exp\left[-1268\left(\frac{1}{303}-\frac{1}{T_{fc}}\right)\right] \approx 0 \tag{28}$$

Solving equation (28) for λ, an estimation of the inner water content of the reference impedance can be obtained. Moreover, equation (24) can be further combined with equation (27) leading to:

$$I_L \approx I + \frac{\bar{\bar{R}}T_{fc}\alpha I}{2\alpha F I\left(R_{LF} - R_{HF}\right) - \bar{\bar{R}}T_{fc}} \tag{29}$$

Since the equivalent resistance of the reference impedance can be evaluated from R_{LF} (see equation (26)), the water content and limiting current density values estimated through equation (28) and (29) are fundamental for the correct estimation of the stack equivalent resistance $R_{eq,stk}$ in equation (14). Indeed, the impedance scaling is performed by introducing reasoned physical assumptions on water content and limiting current distributions within the stack. It is here assumed that, for a stack made of N_c cells, the first cell shows the following values:

$$\lambda_{C_1} = \lambda\left(1 + \Delta\lambda_{C_1}\right) \tag{30a}$$

$$I_{L,C_1} = I_L\left(1 + \Delta I_{L,C_1}\right) \tag{30b}$$

whereas the last cell shows:

$$\lambda_{C_{N_c}} = \lambda\left(1 + \Delta\lambda_{C_{N_c}}\right) \tag{31a}$$

$$I_{L,C_{N_c}} = I_L\left(1 + \Delta I_{L,C_{N_c}}\right) \tag{31b}$$

Introducing a linear distribution of such parameters within the stack, the i-th cell shows the following internal properties:

$$\lambda_{C_i} = \frac{\lambda_{C_{N_c}} - \lambda_{C_1}}{N_c - 1}\left(i - 1\right) + \lambda_{C_1} \tag{32a}$$

$$I_{L,C_i} = \frac{I_{L,C_{N_c}} - I_{L,C_1}}{N_c - 1}\left(i - 1\right) + I_{L,C_1} \tag{32b}$$

From these values shown in equations (30) through (32), equations (15) through (19) and (24) can be used to evaluate the equivalent resistance of the i-th cell R_{eq,C_i}. Afterwards, the overall equivalent stack resistance is computed as:

$$R_{eq,stk} = \sum_{i=1}^{N_c} R_{eq,C_i} \tag{33}$$

and the scaled-up impedance is evaluated through equation (14).

4. Results and discussion on scaling-up approach application

To verify the consistency and the validity of the proposed scaling-up methodology, different impedance spectra have been accounted, taken from the literature [32] and measured within the framework of the European Project HEALTH-CODE [33]. To resume and clearly define all the required steps for the methodology application, a summarizing scheme is presented in Figure 1.

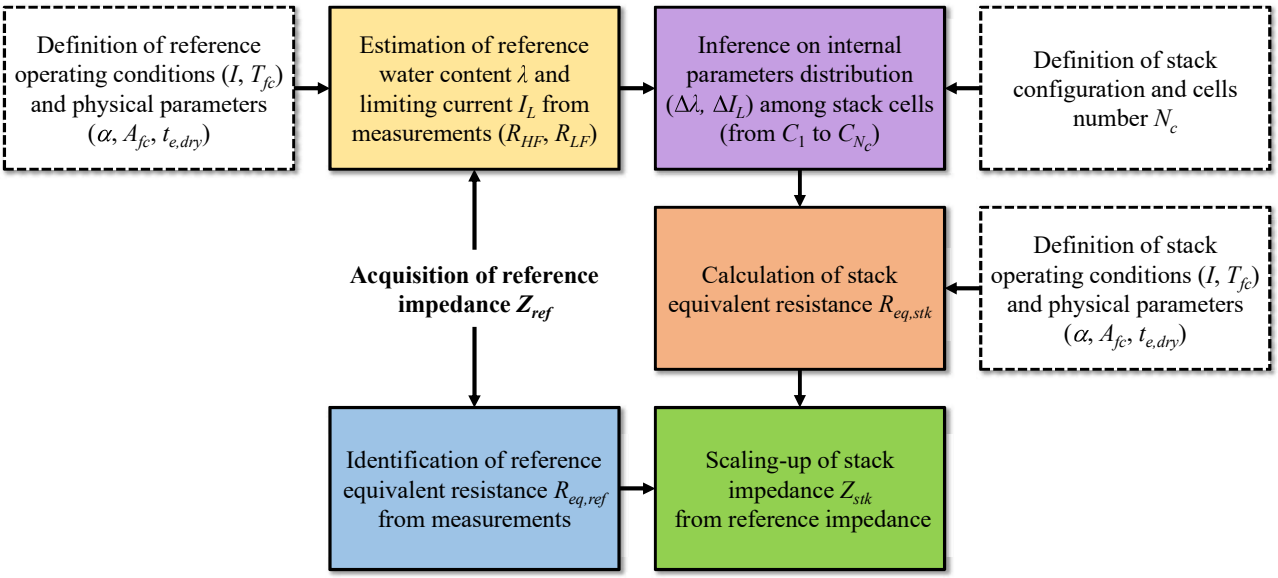

Figure 1 – Schematic representation of the logical methodology application for the scaling-up of PEMFC stack impedance.

As first analysis, a comparison with the experimental data presented by Westerlain et al. [32] is performed. This investigation allows proving the consistency of approach with respect to the results already presented by the authors in [24]. The reference and stack operating conditions and physical parameters needed for impedance scaling-up (as recalled in the scheme of Figure 1) are illustrated in Table 1.

The stack tested by Wasterlain et al. [32] is made of 20 cells in counter-flow configuration, with hydrogen flow in opposition to air and cooling flows. The reference cell considered for stack impedance scaling-up is the 20th cell, located at the hydrogen outlet (and air and cooling inlet). According to what described in [32], cell 20 experienced a lower performance, showing a greater diffusion arc. Therefore, the simple scaling-up that can be achieved by multiplying cell impedance by the cells number is not effective, and a physical reasoning on parameters distribution within the stack is necessary.

Table 1 – Operating conditions and physical parameters of reference and stack impedances related to the data presented by Wasterlain et al. [32].

Parameter	Reference Value	Stack Value
Operating temperature T_{fc}	80°C	80°C
Operating current I	50 A	50 A
Cells number N_c	1	20
Dry electrolyte thickness $t_{e,dry}$	~130 µm	~130 µm
Fuel cell area A_{fc}	100 cm^2	100 cm^2
Charge transfer coefficient α	0.5	0.5

The reference impedance of cell 20 is shown in Figure 2, with blue line and circle markers. On the same figure, the high frequency and low frequency resistance intercepts (R_{HF} = 1.3 mΩ and R_{LF} = 11.1 mΩ) are also presented with red markers. By means of such significant points, cell water content and limiting current can be evaluated through equations (28) and (29), respectively, obtaining λ = 13 and I_L = 51.7 A.

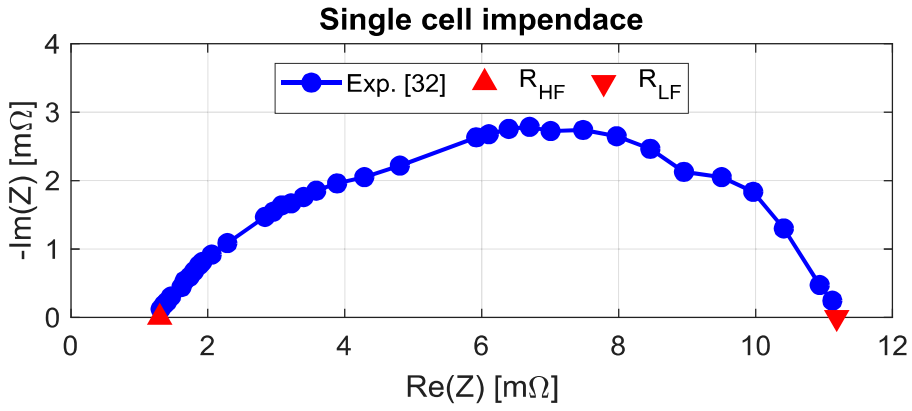

Figure 2 – Single cell impedance spectrum related to the 20th cell of the PEMFC stack tested by Wasterlain et al. [32], with high frequency and low frequency intercepts with the real axis (R_{HF} and R_{LF}, respectively).

The reference cell is practically the last cell of the stack, and it can be assumed that $\Delta\lambda_{C_{N_c}} = \Delta I_{L,C_{N_c}} = 0$. According to its location, the cell may experience several problems, such as lower fuel utilization (since the

hydrogen concentration approaching the outlet is lower) and higher water concentration with respect to anode inlet side, as also commented in [32]. Such information allows different assumptions on the water content and liming current distribution within the stack. The first cell is at the opposite location with respect to the reference cell (i.e., at hydrogen inlet and air and cooling outlet), experiencing higher fuel utilization and a better humidification (since more water is usually present at cathode outlet), which implies higher water content and limiting current. Assuming an increase in the water content of 3% and an increase in limiting current of 8%, it can be defined $\Delta\lambda_{C_1} = +0.03$ and $\Delta I_{L,C_1} = +0.08$, with $\lambda_{C_1} = 14$ and $I_{L,C_1} = 55.8$ A. The obtained average water content and limiting current within the stack are 13.1 and 53.7 A, respectively.

Recalling the values reported in Table 1 and the procedure illustrated in Figure 1, the overall stack impedance can be scaled up. The reference cell impedance is that shown in Figure 2, while the reference equivalent resistance is equal to the identified value of R_{LF}. The stack equivalent resistance $R_{eq,stk}$ is evaluated through the equations presented in the previous section, obtaining a value of 128 mΩ. Hence, the final stack impedance Z_{stk} can be achieved through equation (14). The obtained results are presented in Figure 3, with the scaled-up impedance represented with red line and square markers. The comparison is made with respect to the experimental data of Wasterlain et al. [32], in blue line and circle markers, and the overall impedance obtained by multiplying the cell impedance by the number of cells (in black line and diamond markers).

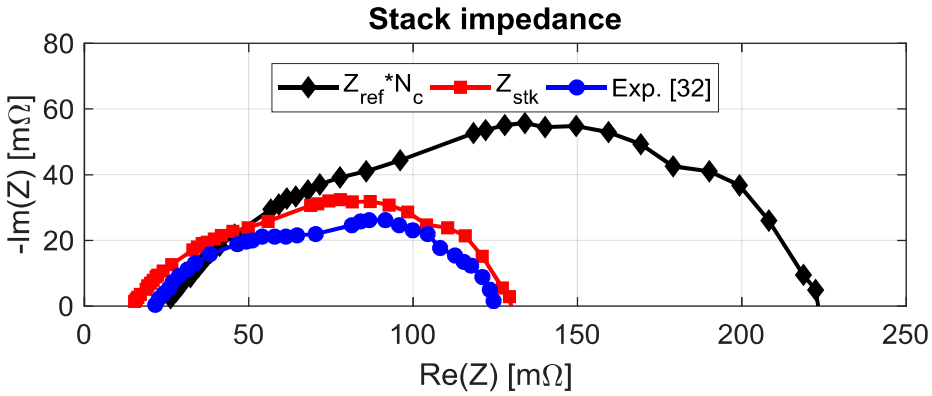

Figure 3 – Comparison of the scaled-up stack impedance Z_{stk} (red line with square markers) with the experimental data of Wasterlain et al. [32] (blue line and circle markers) and the cell spectrum multiplied by the number of cells (black line and diamond markers).

It can be noted that the scaled-up impedance Z_{stk} shows a good similarity with the experimental data, in consistency with the result presented in [24] and [25]. As already commented, the simple scaling-up obtained by multiplying cell impedance with cells number does not provide an effective representation of stack impedance, thus proving the need for suitable physical reasoning.

To prove the robustness of the approach, further impedance spectra, acquired within the framework of the HEALTH-CODE project [33], have been considered for scaling-up purposes. Such data refer to a stack provided by Ballard Power System Europe A/S and tested by the European Institute for Energy Research. This stack is made of 46 cell in counter-flow configuration and tested under different operating conditions. The main operational and physical parameters accounted for the present study are listed in Table 2 for two particular cases, which only differ for the imposed current: Case #1 relates to an operating current of 40 A, whereas Case #2 to an operating current of 15 A.

Table 2 – Operating conditions and physical parameters of reference and stack impedances related to the data acquired within the HEALTH-CODE project [33]; two main operating currents are considered, Case #1 with 40 A and Case #2 with 15 A.

Parameter	Case #1		Case #2	
	Reference Value	Stack Value	Reference Value	Stack Value
Operating temperature T_{fc}	57°C	57°C	57°C	57°C
Operating current I	40 A	40 A	15 A	15 A
Cells number N_c	1	46	1	46
Dry electrolyte thickness $t_{e,dry}$	~130 μm	~130 μm	~130 μm	~130 μm
Fuel cell area A_{fc}	100 cm^2	100 cm^2	100 cm^2	100 cm^2
Charge transfer coefficient α	0.5	0.5	0.5	0.5

For each case, three different single cell impedances have been measured and tested for stack impedance scaling-up, and are related to the first (Cell #1), middle (Cell #23) and last (Cell #46) cells of the stack. The first cell is located at the air inlet/hydrogen outlet, while the last one at the air outlet/hydrogen inlet. It is straightforward to understand that, for each cell impedance, specific physical assumptions on internal

parameters distribution should be made according to its location. Following the scheme presented in Figure 1, the main reference and physical parameters for the scaling-up procedure are listed in Table 3.

Table 3 – Main reference and physical parameters accounted for scaling-up procedure for Case #1 and Case #2 listed in Table 2, with first (Cell #1), middle (Cell #23) and last (Cell #46) cells of the stack taken as reference cells, respectively.

Parameter	Case #1			Case #2		
	Cell #1	Cell #23	Cell #46	Cell #1	Cell #23	Cell #46
λ	17.0	17.9	20.6	19.0	19.2	22.0
I_L	47.8 A	45.2 A	44.8 A	18.9 A	18.1 A	18.1 A
$R_{eq,ref}$	3.6 mΩ	4.4 mΩ	4.5 mΩ	6.4 mΩ	7.3 mΩ	7.1 mΩ
$\Delta\lambda_{C_1}$	0	-0.01	-0.26	0	-0.01	-0.26
$\Delta\lambda_{C_{N_c}}$	+0.05	+0.02	0	+0.03	+0.01	0
$\Delta I_{L,C_1}$	0	+0.01	+0.03	0	+0.03	0
$\Delta I_{L,C_{N_c}}$	-0.09	-0.01	0	-0.08	-0.03	0
average λ_{stk}	17.8	18.0	18.0	19.3	19.2	19.1
average $I_{L,stk}$	45.5 A	45.2 A	45.1 A	18.2 A	18.1 A	18.1 A
$R_{eq,stk}$	195.2 mΩ	195.0 mΩ	188.8 mΩ	332.3 mΩ	331.2 mΩ	329.6 mΩ

The water content λ and limiting current I_L values listed in this table have been evaluated through significant points identification on cell impedance spectrum (in the same way as illustrated in Figure 2) and using equations (28) and (29), respectively. The reference equivalent resistance $R_{eq,ref}$ values are instead obtained through equation (26) upon identification of R_{LF}. The water content and limiting current variations of the first (C_1) and last (C_{N_C}) cells with respect to the reference ones have been assumed considering the location of this latter: for Cell #1 it is always assume that $\Delta\lambda_{C_1} = \Delta I_{L,C_1} = 0$, whereas for Cell #46 it is imposed $\Delta\lambda_{C_{N_c}} = \Delta I_{L,C_{N_c}} = 0$. Obviously, the middle cell has different internal parameters values with respect to the first and last cells.

To set the other variations, the following physical considerations are made: (i) no fuel utilization issues are considered (i.e., no hydrogen depletion is accounted for the cells at hydrogen outlet), and (ii) the main

losses are related to water management issues (i.e., flooding and dehydration). Therefore, the cell located at air inlet/hydrogen outlet (Cell #1) may experience lower water concentration with respect to the last cell located air outlet/hydrogen inlet. This means that the last cell shows a higher water content (more water is accumulated at air outlet) with consequent increase in transport losses (i.e., with lower limiting current). The opposite comments can be made when analyzing Cell #46. Upon definition of the internal parameters distribution, the average water content and limiting current values of the stack are reported in Table 3, with also the corresponding values of the stack equivalent resistance $R_{eq,stk}$. By means of such values, the scaling-up of the stack impedance is achieved and all the results for the two cases and the three reference single cells are presented in Figure 4. As done for the data of [32], the proof of the scaling-up approach validity is made comparing the scaled-up stack impedance with the measured one and with the impedance obtained by multiplying the reference cell impedance with the cells number. The scaled up impedances Z_{stk} are represented in red lines and square markers, the experimental data in blue lines and circle markers, while the cell impedances multiplied by the cells number are represented with black lines and diamond markers.

From an overall point of view, it can be stated that the scaling-up procedure gives very good results in terms of stack impedance representation, being always superimposed to the experimental one. More in details, it can be stated that the first cell always shows higher limiting current and lower water content with respect to the stack average, obtaining a lower spectrum if merely multiplied by the cells number. Conversely, the last cell shows a larger spectrum when multiplied by cells number, since it experiences a higher water content and lower limiting current (i.e., higher losses). Instead, the middle cell is generally representative of the stack behavior, as also confirmed by the achieved results.

The results here illustrated proved the validity of the proposed scaling-up approach under use of experimental data from different sources. The methodology proved being consistent and accurate, even though simplifying assumptions on the distribution of key internal state variables have been introduced. The introduction of a more detailed modelling framework with respect to what presented by the authors in [24] and [25] did not reduce approach robustness and accuracy. It can be further stated that the reduced complexity achieved via non-dimensional analysis can significantly improve online applications related to monitoring, diagnostic and control [34][35][36], upon the extension of the scaling-up procedure to faulty cells/stacks [37] and through suitable models accounting for degradation phenomena.

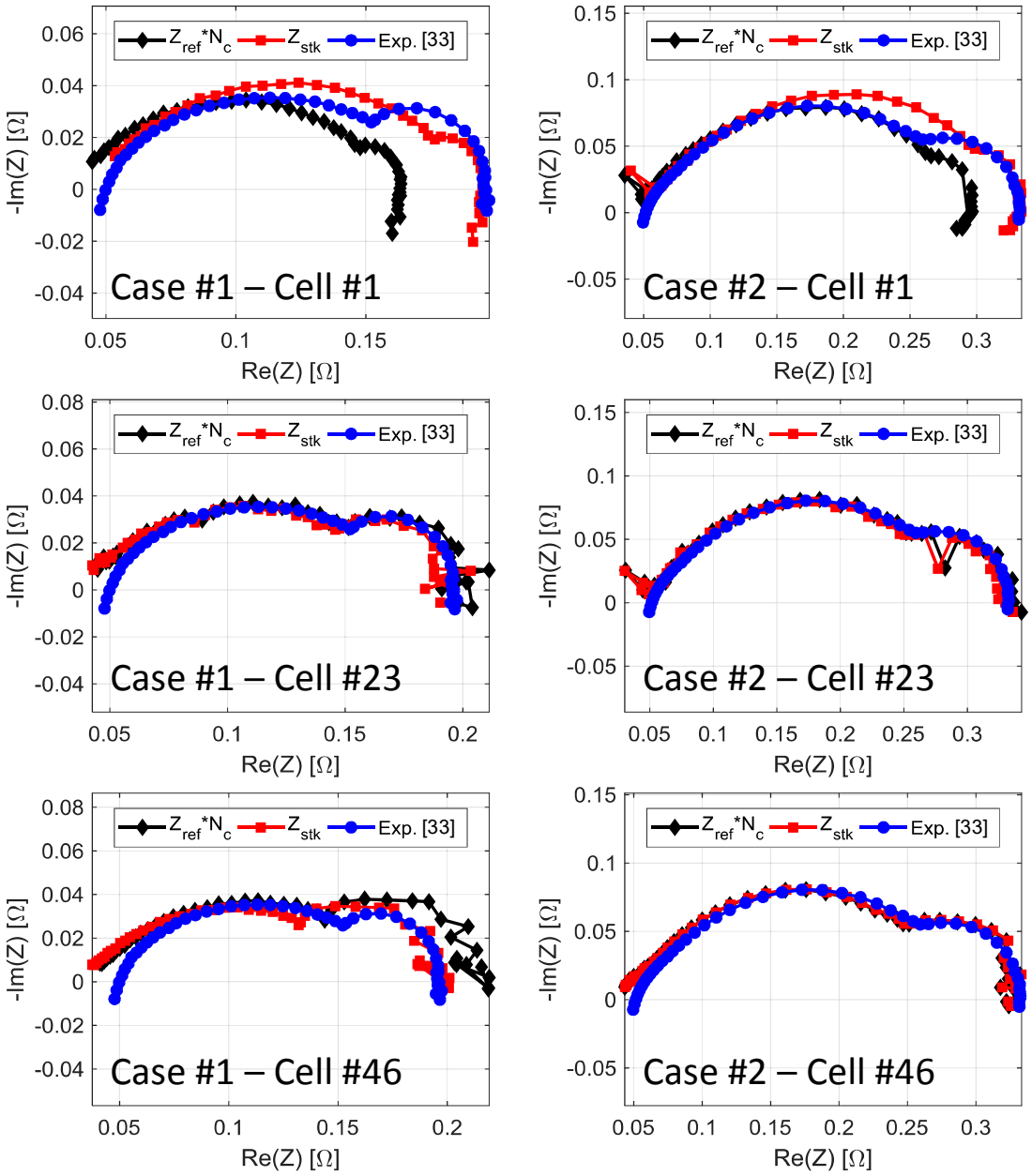

Figure 4 – Comparison of the scaled-up stack impedance Z_{stk} (red line with square markers) with the experimental data of the HEALTH-CODE project [33] (blue line and circle markers) and the cell spectrum multiplied by the number of cells (black line and diamond markers); each row refers to first (Cell #1), middle (Cell #23) or last (Cell #46) cell and each column to Case #1 or Case #2, respectively.

5. Conclusions

The present paper discussed the improvements concerning a scaling-up methodology for Proton Exchange Membrane Fuel Cell (PEMFC) impedance. The Buckingham Pi theorem has been considered as basis for methodology design and impedance modelling, with two main innovations with respect to the

available literature: (i) a generalized model based on a more phenomenological approach is applied for non-dimensional parameters computation, reducing the need for experimental data; (ii) the evaluation of cell internal states is performed through parameters extraction from reference cell impedance measurement. Concerning the first point, a physical representation of the relationship between polarization resistance and limiting current has been established through voltage losses modelling and derivative. With respect to the second point, the estimation of cell water content and limiting current are performed by means of inverse modelling based on high and low frequency resistances of the measured cell impedance. Detailed assumptions on internal parameters distribution within the stack has been identified as significant aspects for successful methodology application. The capabilities and accuracy of the scaling-up approach has been tested on different experimental data, also proving its robustness and remarking the needs for proper physical assumptions. Each stack impedance has been accurately reproduced through the use of only a single cell spectrum. Future works will entail assessing algorithm validity on further experimental data as well as stack/cell sizes. Moreover, an improved modelling framework is also considered so as to further distinguish between impedance real and imaginary parts and to apply the algorithm on other technologies, such as Solid Oxide Fuel Cells.

Acknowledgements

The research leading to these results has received funding from the University of Salerno and from the Fuel Cells and Hydrogen 2 Joint Undertaking under grant agreement No 671486 (project HEALTH-CODE - Real operation pem fuel cells HEALTH-state monitoring and diagnosis based on dc-dc COnverter embeddeD Eis). This Joint Undertaking receives support from the European Union's Horizon 2020 research and innovation programme and from Italy, Denmark, Germany and France.

References

[1] Facci, A.L., Ubertini, S., Analysis of a fuel cell combined heat and power plant under realistic smart management scenarios (2018) Applied Energy, 216, pp. 60-72.

[2] Sankar, K., Jana, A.K., Nonlinear multivariable sliding mode control of a reversible PEM fuel cell integrated system (2018) Energy Conversion and Management, 171, pp. 541-565.

[3] Song, K., Li, F., Hu, X., He, L., Niu, W., Lu, S., Zhang, T., Multi-mode energy management strategy for fuel cell electric vehicles based on driving pattern identification using learning vector quantization neural network algorithm (2018) Journal of Power Sources, 389, pp. 230-239.

[4] Hajjaji, N., Martinez, S., Trably, E., Steyer, J.-P., Helias, A. Life cycle assessment of hydrogen production from biogas reforming (2016) International Journal of Hydrogen Energy, 41 (14), pp. 6064-6075.

[5] U. S. Department of Energy, Fuel Cell Technologies Office Multi-year Research, Development, and Demonstration Plan – 3.4 Fuel Cells (2016) (accessed September 2016).

[6] Fuel Cells and Hydrogen Joint Undertaking, Multi-Annual Work Plan 2014-2020. http://www.fch.europa.eu/page/multi-annual-work-plan (accessed April 2017).

[7] Battelle Memorial Institute, Manufacturing Cost Analysis of 100 and 250 kW Fuel Cell Systems for Primary Power and Combined Heat and Power Applications, U.S. Department of Energy, 2016.

[8] X. Wu, B. Zhou, Fault tolerance control for proton exchange membrane fuel cell systems (2016) Journal of Power Sources, 324, pp. 804-829.

[9] Dijoux, E., Steiner, N.Y., Benne, M., Péra, M.-C., Pérez, B.G., A review of fault tolerant control strategies applied to proton exchange membrane fuel cell systems (2017) Journal of Power Sources, 359, pp. 119-133.

[10] Brunetto C., Moschetto A. and Tina G., PEM fuel cell testing by electrochemical impedance spectroscopy, Electric Power Systems Research (2009), 79, pp. 17-26.

[11] Xie C. and Quan S., Drawing impedance spectroscopy for Fuel Cell by EIS, Procedia Enviromental Sciences (2011), 11, pp. 589-596.

[12] Narjiss A, Depernet D, Candusso D, Gustin F, Hissel D. Online Diagnosis of PEM Fuel Cell. IEEE. 13th Power Electronics and Motion Control Conference (EPE-PEMC) 2008; 734-39.

[13] Kulikovsky, A.A., Analytical physics-based impedance of the cathode catalyst layer in a PEM fuel cell at typical working currents, Electrochimica Acta 225 (2017) 559-565.

[14] Kulikovsky, A.A., A simple physics-based equation for low-current impedance of a PEM fuel cell cathode, Electrochimica Acta 196 (2016) 231-235.

[15] Kulikovsky, A.A., PEM Fuel Cell Impedance at Open Circuit, Journal of The Electrochemical Society, 163 (5) F319-F326 (2016).

[16] Cruz-Manzo, S., Perezmitre-Cruz, C., Greenwood, P., Chen, R., An impedance model for analysis of EIS of polymer electrolyte fuel cells under platinum oxidation and hydrogen peroxide formation in the cathode, Journal of Electroanalytical Chemistry 771 (2016) 94-105.

[17] Niya, S.M.R., Phillips, R.K., Hoorfar, M., Process modeling of the impedance characteristics of proton exchange membrane fuel cells, Electrochimica Acta 11 (2016) 594-605.

[18] Setzler, B.P., Fuller, T.F., A Physics-Based Impedance Model of Proton Exchange Membrane Fuel Cells Exhibiting Low-Frequency Inductive Loops, Journal of The Electrochemical Society, 162 (6) F519-F530 (2015).

[19] Chevalier, S., Auvity, B., Olivier, J.C., Josset, C., Trichet, D., Machmoum, M., Detection of Cells State-of-Health in PEM Fuel Cell Stack Using EIS Measurements Coupled with Multiphysics Modeling (2014) Fuel Cells, 14, 416-429.

[20] Chevalier, S., Trichet, D., Auvity, B., Olivier, J.C., Josset, C., Machmoum, M., Multiphysics DC and AC models of a PEMFC for the detection of degraded cell parameters, International Journal of Hydrogen Energy, 38 (2013), 11609-11618.

[21] Pahon, E., Yousfi Steiner, N., Jemei, S., Hissel, D., Moçoteguy, P., A signal-based method for fast PEMFC diagnosis, Applied Energy 165 (2016) 748-758.

[22] Zunyan Hu, Liangfei Xu, Yiyuan Huang, Jianqiu Li, Minggao Ouyang, Xiaoli Du, Hongliang Jiang, Comprehensive analysis of galvanostatic charge method for fuel cell degradation diagnosis (2018) Applied Energy, 212, 1321-1332

[23] Petrone R., Pianese C., Polverino P., Sorrentino M., International Patent Application no. PCT/IB2015/058258 claiming the priority of the Italian Patent Application no. RM2014A000641, entitled "Method For Monitoring And Diagnosing Electrochemical Devices Based On Automatic Electrochemical Impedance Identification", 2014.

[24] Russo L., Sorrentino M., Polverino P., Pianese C., Application of Buckingham π theorem for scaling-up oriented fast modelling of Proton Exchange Membrane Fuel Cell impedance, Journal of Power Sources 353 (2017) 277-286.

[25] Polverino P., Bove G., Sorrentino M., Pianese C., Generalized scaling-up approach based on Buckingham theorem for Polymer Electrolyte Membrane Fuel Cells impedance simulation, Energy Procedia (under publication).

[26] Kline, S.J., Similitude and Approximation Theory, Springer-Verlag, 1986.

[27] National Institute of Standards and Technology, The International System of Units (SI), NIST Special Publication 330, B.N. Taylor & A. Thompson, 2008.

[28] Massey, B., Mechanics of Fluids, Eight Edition, Taylor & Francis, 2006.

[29] Springer T.E., Zawodzinski T.A., Gottesfeld S., Polymer Electrolyte Fuel Cell Model, Journal of the Electrochemical Society 138 (8) (1991) 2334-2342.

[30] Ferrara, A., Polverino, P., Pianese, C., Analytical calculation of electrolyte water content of a Proton Exchange Membrane Fuel Cell for on-board modelling applications, Journal of Power Sources 390 (2018) 197-207.

[31] Larminie J., Dicks A., Fuel Cell Systems Explained, Second Edition, Wiley, 2003.

[32] Wasterlain S., Candusso D., Harel F., Hissel D., François X., Development of new test instruments and protocol for the diagnostic of fuel cell stacks, Journal of Power Sources 196 (2011) 5325-5333.

[33] HEALTH-CODE, http://pemfc.health-code.eu/ (visited on January 2019).

[34] Dotelli, G., Ferrero, R., Stampino, P.G., Latorrata, S., Toscani, S., Low-cost PEM fuel cell diagnosis based on power converter ripple with hysteresis control, IEEE Transactions on Instrumentation and Measurement 64 (2015), 2900-2907.

[35] Polverino, P., Pianese, C., Model-based prognostic algorithm for online RUL estimation of PEMFCs, Proceedings of the 2016 3rd Conference on Control and Fault-Tolerant Systems (SysTol), Barcelona, Spain, Sept. 7-9, 2016, pp. 599-604.

[36] Polverino, P., Frisk, E. Jung, D., Krysander, M., Pianese, C., Model-based diagnosis through Structural Analysis and Causal Computation for automotive Polymer Electrolyte Membrane Fuel Cell systems, Journal of Power Sources 357 (2017) 26-40.

[37] Petrone, R., Vitagliano, C., Péra, M.C., Chamagne, D., Sorrentino, M., Characterization of an H2/O2 PEMFC Short-Stack Performance Aimed to Health-State Monitoring and Diagnosis, Fuel Cells 18 (2018) 279-286.